Study on Flow Boiling Heat Transfer in Segmented Internally-Threaded Tube

J. Yang, Y. J. Xiao, Q. He, J. Y. Cheng, Y. S. Zhang and H. W. Jia[†]

College of Environmental Science and Engineering, Donghua University, Shanghai 201620, China

†*Corresponding Author Email: jiahw@dhu.edu.cn*

ABSTRACT

The flow boiling heat transfer characteristics of R245fa in segmented internally-threaded tubes are studied experimentally. The heat transfer performances of smooth tube, front-threaded tube, rear-threaded tube, and full-threaded tube are compared. The experiments are carried out with heat flux ranging from 14.01 to 48.79 kW·m-2 and mass flux ranging from 125 to 375 kg·m-2·s-1. The experimental results show that the internal thread structure facilitates the heat transfer. At low mass fluxes and low heat fluxes, the heat transfer performance of the full-threaded tube is the best, while at high heat fluxes and high mass fluxes, that of the front-threaded tube is the best. Convective boiling is dominant in the smooth tube and the front-threaded tube, and corresponding heat transfer coefficients increase significantly with increasing mass flux. In contrast, nucleate boiling dominates in the rear- and full-threaded tube, and the heat transfer coefficients almost keep unchanged with increasing mass flux. The front- and rear-threaded tubes exhibit significantly different heat transfer characteristics, although they have the same heat transfer area. The effect of convective perturbation and bubble nucleation caused by the internal thread structure varies with the zone and intensity, leading to the change of the dominant mechanism of boiling heat transfer.

Key words: Flow boiling; Segmented internally-threaded tube; Dominant mechanism; Heat transfer characteristic; Experiment.

NOMENCLATURE

A_f	cross-sectional area		T	measuring temperature value
γ	top angle of thread tooth		T	temperature
β	thread helix angle		U	voltage
c_p	isobaric specific heat capacity		I	enthalpy
D_h	equivalent inner diameter		x	vapor quality
D_{in} D_{out}	inner diameter and outer diameter of test tube		ε	heating efficiency
EF	Enhancement Factor		λ	thermal conductivity
G	mass flux			
H	thread top height		**Subscripts**	
h	heat transfer coefficient		i	position mark of measuring point
I	current		in	import
M	mass flow rate		out	export
MAE	Mean Absolute Error		w	wall shear
MF	Merit Factor		l	liquid state
m	mass flow rate		v	gaseous state
PF	Penalty Factor		ave	average value
p	measuring pressure value		exp	experimental value
Q	output power		pre	predicted value
q	heat flux		sat	saturation value

1. INTRODUCTION

Flow boiling is widely used in refrigeration and air conditioning, industrial boiler, nuclear reactors, and other fields for its excellent heat transfer performance (Hao *et al.* 2020). Compared with the smooth tube used in the traditional two-phase heat transfer system (Ali *et al.* 2012; Charnay *et al.* 2014; Mendoza *et al.* 2016; Feng *et al.* 2022), the micro-fin tube could significantly improve the heat transfer performance. Therefore, the research on the flow boiling in the micro-fin tube has attracted much attention (Seo and Kim 2000; Solanki and Kumar 2018; Dastmalchi *et al.* 2017; Jiang *et al.* 2017). For example, He *et al.* (2016) have compared the flow boiling heat transfer coefficients (HTCs) of various refrigerants (i.e., R410A, R290 and R32/R290) in smooth tubes and micro-fin tubes with different inner diameters (IDs) of 5 mm, 7 mm and 9.52 mm respectively. The experimental results showed that the heat transfer performances in micro-fin tubes would be much better. Solanki and Kumar (2018) have also made comparisons between smooth straight tube and micro-fin helical coiled tube, and the HTC and the frictional pressure drop of the latter were both higher than that of the former. Jiang *et al.* (2016) studied the boiling heat transfer of four refrigerants (i.e., R22, R134a, R407C and R410A) and found that under the same conditions (i.e., same mass flux, pressure drop and power consumption), the efficiency index of the micro-fin tube was higher than that of the smooth tube. Liang *et al.* (2019) investigated the boiling heat transfer and pressure drop characteristics of R410A in a 5 mm internally-threaded tube. The HTC of the threaded tube was higher and was found to increase only with increasing heat flux, while the pressure drop would increase with the increasing mass flux and heat flux.

To describe the difference of heat transfer and pressure drop characteristics of the micro-fin tube versus the smooth tube, Targanski and Cieslinski (2007) defined the ratio of the boiling heat transfer coefficient between the micro-fin tube and the smooth tube as an enhancement factor (i.e., EF), and proposed the ratio of the pressure drop between the micro-fin tube and the smooth tube as penalty factor (i.e., PF). Moreover, a merit factor (MF=EF/PF) was also developed to characterize the comprehensive performance. In the study of Filho and Jabardo (2014), these parameters were used to analyze the performance of herringbone and threaded tubes. It was found that EF would increase with the Reynolds number (*Re*), and MF values for both tubes were less than 1. This indicated that the increase in HTC was accompanied by a significant lift in pressure drop for both types of tubes, i.e., a significant rise in flow resistance.

Scholars have also managed to find the reasons why micro-fin tubes could enhance the flow boiling heat transfer. In the study of He *et al.* (2019), the internal thread structure was found to promote the disturbance of refrigerant, reduce the thickness of the liquid film and enhance the heat transfer, but also increase the frictional resistance of the working fluid in the tube. Moreover, the increase in heat transfer area was considered as another important reason for heat transfer enhancement in the study of Yang and Hrnjak (2018). Their visualization results have also shown that the bubble behavior in the tube was significantly affected by the micro-fin geometry, which was confirmed by recent studies (Yang and Hrnjak 2019, 2020a, b). In addition, Filho and Jabardo (2014), after comparing the heat transfer characteristics of different tubes including herringbone, micro-fin, and smooth tubes, concluded that the heat transfer enhancement was also related to the secondary flow caused by the micro-fin structure.

The effect of the structural parameters of the micro-fin on the flow boiling heat transfer has been the focus of existing studies. Dastmalchi *et al.* (2017) have investigated the influence of the fin height and spiral angle and found that the convective heat transfer was enhanced with the increase of the fin height. In addition, there was an optimal spiral angle with the best heat transfer performance. In the study of Ding *et al.* (2020), the heat transfer in a micro-fin tube with an inner diameter of 5 mm was studied, and the HTCs were found to increase significantly with the increasing tooth height and helix angle. Ma *et al.* (2011) compared the boiling heat transfer characteristics of three internally-threaded tubes with different helix angles and wing heights, and found that the tube with a helix angle of 18° ~ 25° and wing height of no more than 2 mm presented the best heat transfer capacity. Ouyang *et al.* (2015) investigated the flow boiling in three enhanced tubes with different thread structures. The results showed that a larger spiral angle was conducive to heat transfer in laminar flow or transition flow, while in annular flow, a larger number of threads was more beneficial for heat transfer.

It can be seen that existing studies have typically used a single form of micro-fin distribution and have found that the use of micro-fin tubes significantly improves the heat transfer capacity but increases the flow resistance. Therefore, the present study proposes a segmented combination form of internally-threaded and smooth tubes, aiming to improve the comprehensive performance. The effects of the segmented distribution on the flow boiling heat transfer are investigated in detail, and the corresponding heat transfer mechanisms are studied.

2. EXPERIMENTAL SET-UP

2.1 Test Rig

The experimental system is mainly composed of refrigerant circulation and cooling water circulation, and the schematic diagram is shown in Fig. 1. In the cooling water circulation, the working fluid is cooled by a thermostatic water tank (DC-2020) and a condenser consisting of a plate heat exchanger. The refrigerant cycle mainly consists of a gear pump (GAFST23.JDS.A-S2), a Coriolis flowmeter (DMF-1-1A), a preheating section (TDGC2-0.2kVA), a test section, and a reservoir. Here, the gear pump drives the refrigerant flow, and the Coriolis flowmeter is used to measure the mass flow rate instantly. The preheating section is composed of a copper tube with a heating wire uniformly wound on its outer surface.
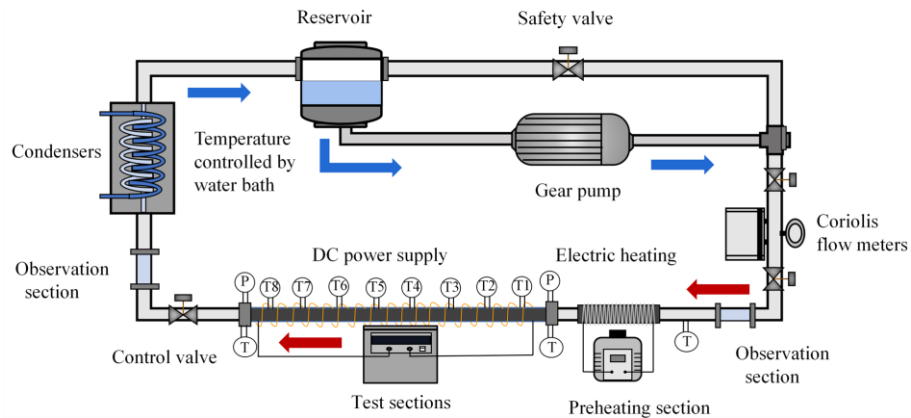
Fig. 1. Schematic diagram of the experimental system.

Thereby, the sub-cooling of the refrigerant at the inlet of the test section could be changed by adjusting the applied heating power. The reservoir is used to collect the refrigerant and complete gas-liquid separation. All the experimental setups are covered with insulation foam to minimize heat leakage. The experimental data, such as temperature, pressure, and mass flow rate are recorded and stored in the computer using a data acquisition device (Agilent 34972a).

2.2 Test Section

The test section is mainly composed of a copper tube with a length of 700 mm. Two flange structures are welded to the inlet and outlet of the tube, and embedded thermocouples and pressure sensors are installed to measure the temperature and pressure of the refrigerant in the system. Eight temperature measuring points are set equidistantly along the flow direction on the outer wall of the test tube. In addition, three T-type thermocouples are arranged at each measuring point, located at the top, middle and bottom with an interval of 90°. In the present study, four types of tubes are studied, which are smooth tube, full-threaded tube, front-threaded tube and rear-threaded tube, as shown in Fig. 2. The corresponding structural parameters are given in Table 1. The working fluid used is R245fa. Finally, the flow boiling heat transfer characteristics of R245fa under the conditions of heat flux of 7.98~55.53 kW·m^{-2} and mass flow rate of 125~375 kg·m^{-2}·s^{-1} in four kinds of tubes could be studied. Fig. 2(e) shows the schematic diagram of the internal thread structure. D_{in} and D_{out} are the inner and outer diameters of the test tube, respectively, L is the tube length, H is the fin height, N is the number of threads, W is the rib pitch, β is the helix angle, δ is the rib fin width, γ is the tooth apex angle, and the relevant structural parameters are listed in Table 1.

3. DATA DEDUCTION

3.1 Data Treatment

The effective heat (Q_{eff}) applied on the test section can be obtained by multiplying the output power (Q) and the heating efficiency (ε):

(a) Smooth tube

(b) Front-threaded tube

(c) Rear-threaded tube

(d) Full-threaded tube

(e) Internal thread structure
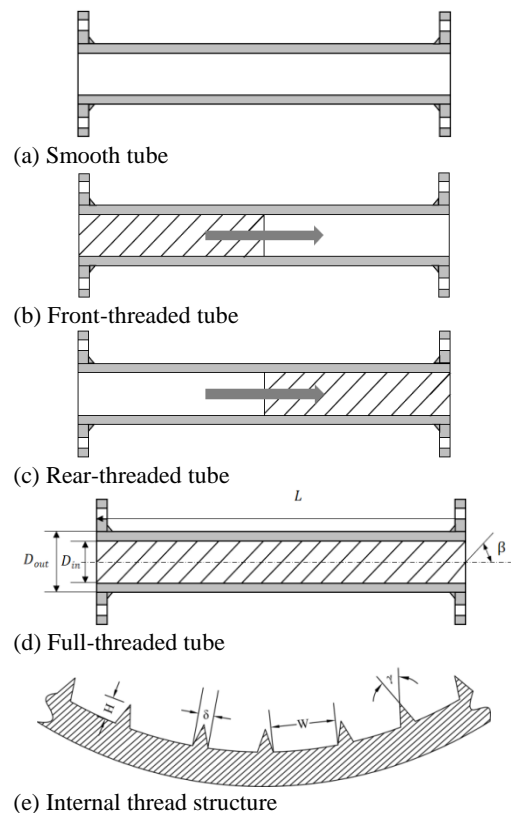
Fig. 2. Tube type of the test sections.

Table 1 Dimensions of the testing tubes

Types	Smooth tube	Full-threaded tube	Segmented tube	
			Threaded tube	Smooth tube
D_{out}/ mm	5	5	5	5
D_{in}/mm	4.3	4.6	4.6	4.3
L/mm	700	700	350	350
H/mm	—	0.14	0.14	—
N	—	38	38	—
W/mm	—	0.28	0.28	—
β/°	—	18	18	—
δ/mm	—	0.1	0.1	—
γ/°	—	40	40	—

$$Q_{\text{eff}} = \varepsilon Q \tag{1}$$

where ε could be estimated by single-phase heat transfer experiments (Liu *et al*. 2020). Subsequently, the heat flux of the test section can be obtained:

$$q = \frac{Q_{\text{eff}}}{\pi D_{\text{h}} L} \tag{2}$$

where D_h is the equivalent inner diameter of the test tube (Zhao and Bansal 2012):

$$D_{\text{h}} = \sqrt{\frac{4A_{\text{c}}}{\pi}} \tag{3}$$

where A_C is the inner cross-sectional area. Besides, it can be calculated as follows when there are internal thread structures:

$$A_{\text{c}} = \frac{\pi D_{\text{in}}^2}{4} - N \cdot A_{\text{f}} \tag{4}$$

where A_f represents the cross-sectional area of a single fin.

According to Newton cooling formula, the heat transfer coefficient can be obtained:

$$h_{\text{exp}} = \frac{q}{(T_{\text{w,in}} - T_{\text{sat}})} \tag{5}$$

where $T_{\text{w,in}}$ is the inner wall temperature of the test tube, and T_{sat} is the saturation temperature of the working fluid. Since the temperature profile along the radial direction of the tube wall approximately satisfies the Fourier law, the temperature of the inner wall can be calculated as follows (Liang *et al*. 2019; Yu *et al*. 2019):

$$T_{\text{w,in}} = T_{\text{w,out}} - \frac{\varepsilon Q \ln(\frac{D_{\text{out}}}{D_{\text{in}}})}{2\pi\lambda L} \tag{6}$$

where λ is the thermal conductivity of the tube wall, which is made of red copper. $T_{\text{w,out}}$ is the outer wall temperature at the measuring point.

The local vapor quality (x_i) is given by:

$$x_{\text{i}} = \frac{(I_{\text{l,in}} + \frac{Q_{\text{eff}}}{m} \times \frac{z_{\text{i}}}{L} - I_{\text{l,i}})}{I_{\text{l,v,i}}} + x_{\text{in}} \tag{7}$$

where $I_{\text{l,in}}$ is the enthalpy of working fluid at the inlet, while $I_{\text{l,i}}$ is the enthalpy of the working fluid at the temperature measuring point; and $I_{\text{l,v,i}}$ is phase change latent heat. Moreover, m is the mass flow rate, z_i is the distance between the measuring point and the inlet, and L is the length of the entire test section.

All the above data processing procedure is implemented by MATLAB programs, where the thermophysical properties involved are obtained by invoking the dynamic database from REFPROP 9.1.

3.2 Uncertainty Analysis

The accuracy of the thermocouples used in the experiment is about $\pm$ 0.2 K, and they have all been calibrated by a standard thermometer. The accuracy of the pressure sensor is $\pm$ 0.25 %, and the uncertainty of output power for the DC power supply is $\pm$ 1.41 %. In addition, the accuracy of the mass flow meter is $\pm$ 0.15 %. The uncertainty of experimental parameters can be estimated by error propagation theory (Moffat 1988).

$$\delta R = \sqrt{\sum_{\text{i}=1}^{\text{n}} \left(\frac{\partial R}{\partial x_{\text{i}}} \delta x_{\text{i}} \right)^2} \tag{8}$$

where δR represents the uncertainty of R (i.e., any main parameters), and δx_i is the uncertainty of x_i. It can be seen that the uncertainty of each variable δx_i would contribute to the overall uncertainty of δR. The uncertainties of the main parameters in the present study are listed in Table 2.

Table 2 Main parameters and their uncertainties

Parameters	Uncertainty
$M/\text{kg}\cdot\text{s}^{-1}$	$\pm$ 0.15 %
$d/(\text{mm})$	$\pm$ 0.02 mm
U/V and I/A	$\pm$ 1 %
T/K	$\pm$ 0.2 K
P/Pa	$\pm$ 0.25 %
$G/\text{kg}\cdot\text{m}^{-2}\cdot\text{s}^{-1}$	$\pm$ 0.94 %
$q/\text{kW}\cdot\text{m}^{-2}$	$\pm$ 1.49 %
$h/\text{kW}\cdot\text{m}^{-2}\cdot\text{K}$	$\pm$ 1.80 %
x	$\pm$ 1.42 %
Q/W	$\pm$ 1.41 %

3.3 Single-phase Experiment

To verify the reliability of the experimental system and to calculate the heating efficiency, single-phase heat transfer experiments with R245fa are conducted first. The sub-cooling of the working fluid at the inlet of the test section is kept near 15°C, and it is ensured that the refrigerant in the test section is single-phase. At this time, the effective heat applied to the test section is equal to the sensible heat change between the inlet and outlet of the working fluid. In turn, the heating efficiency at different heating powers can be obtained, as shown in Fig. 3. It can be seen that the heating efficiency ε of the test section remains at the same level, with an average value of about 87.86 %.
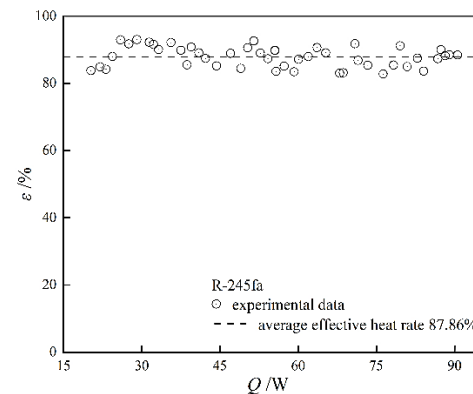

Fig. 3. Heating efficiency of the test section.

The Nusselt numbers (Nu) measured by the single-phase experiment are also compared with the

predicted values of classical empirical correlations (see Table 3). It can be seen that experimental results basically lie between the predicted values of the two correlations when *Re* is less than 3500, as shown in Fig 4(a). When *Re* is larger than 3500, the experimental results would be slightly lower than the prediction of Gnielinski (1975). Fig. 4(b) presents the error analysis between the experimental data and the predicted results of Gnielinski's model, and it can be seen that the experimental data points are within ± 20 % deviation from the predicted values. Overall, the experimental results agree well with the predicted results of Gnielinski's correlation. It confirms that the experimental procedure and data processing in the present study are reasonable, and the experimental setup is reliable.

Table 3 Prediction correlations of Single-phase Heat Transfer

Dittus and Boelter (1985) $Nu_{Dh} = 0.023Re_{Dh}^{0.8}Pr^{0.4}$	$Re > 10000$ $0.6 \leq Pr \leq 160$
Gnielinski (1975) $Nu_{Dh} = \dfrac{(f/8)(Re_{Dh}-1000)Pr}{1+12.7(f/8)^{1/2}(Pr^{2/3}-1)}$ $f = (0.79 \cdot \ln(Re_L)-1.64)^{-2}$	$3000 \leq Re \leq 5\times10^6$ $0.5 \leq Pr \leq 2000$

(a)

(b)
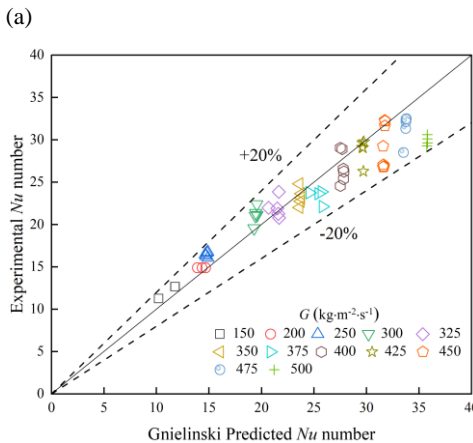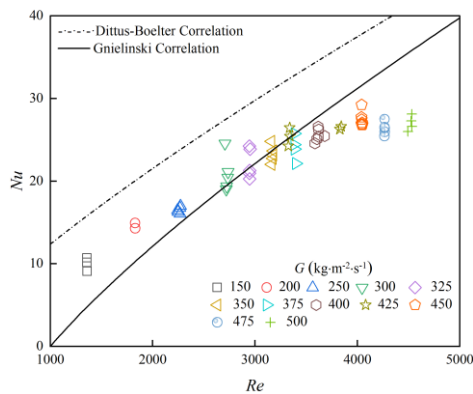
Fig. 4. Comparison of *Nu* of experimental data and predicted values by prediction correlations. (a) Variation of the *Nu* with *Re*. (b) *Nu* error analysis with Gnielinski's correlation.

3.4 Boiling Heat Transfer in Smooth Tube

In addition to the single-phase test, experiments on flow boiling in the smooth tube are also conducted to verify the reliability of the experimental system under boiling conditions. The experimental HTCs are compared with the empirical correlations proposed by Yoshida *et al*. (2011), Liu and Winterton (1991), and Kim and Mudawar (2013) (see Table 4). In addition, the mean absolute error (MAE) between experimental and predicted results is derived:

$$\text{MAE} = \frac{1}{N}\sum \frac{\left|h_{pre}-h_{exp}\right|}{h_{exp}} \times 100\% \qquad (12)$$

**Table 4 Prediction accuracy of empirical correlations for HTC in smooth tube**

Correlations	MAE/%	Data points within 30 %
Yoshida *et al*. (2011)	8.88	98.77 %
Kim and Mudawar (2013)	30.09	51.54 %
Liu and Winterton (1991)	31.91	47.02 %

The comparison of the experimental data with the prediction results of these three correlations is shown in Fig. 5, and the corresponding MAEs are listed in Table 4. It can be seen that the prediction results of Yoshida's correlation have the best agreement with the experimental data. In addition, the corresponding MAE is about 8.88 %, and 98.77 % of the data fall within the error range of ± 30 %, while the MAEs of the other two correlations are larger. Overall, as with the single-phase test, the experimental system also presented good reliability in the flow boiling test.

4. RESULTS AND DISCUSSION

4.1 Comparison of HTCs of Four Types of Tube

Figure 6 shows the variations of average HTCs (i.e., h_{ave}) with the heat flux for the four types of tubes at different mass fluxes. The h_{ave} of the tubes basically increases with the increase of the heat flux, mainly because the increase of heat flux can promote the activation of the nucleate site and the disturbance between the gas phase and liquid phase, thus improving the boiling heat transfer performance (Lu *et al*. 2020). However, it can also be seen that at high heat fluxes, h_{ave} in the smooth tube would decrease slightly when the mass flux is low. This is because local drying occurs in the tube, leading to a decrease in heat transfer coefficient. In addition, there are significant differences in h_{ave} of the smooth tube and the front-threaded tube at different mass fluxes, while the differences between the rear-threaded tube and the full-threaded tube at different mass fluxes are small. Based on the heat transfer characteristics under different dominant boiling mechanisms, i.e., the nucleate boiling and the convective flow boiling (Dorao *et al*. 2018a, 2018b; Subhanker *et al*. 2021; Li *et al*. 2022; Seol *et al*. 2018), it can be found that the boiling heat transfer in the rear-threaded tube and
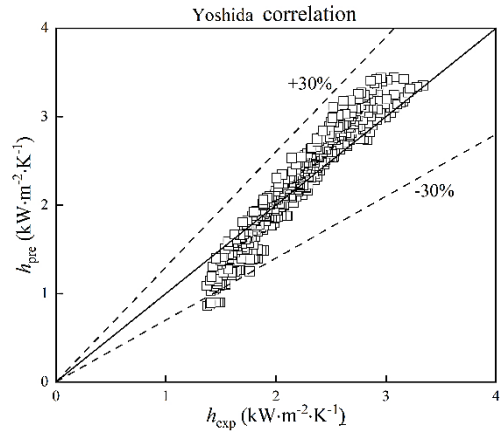
(a)
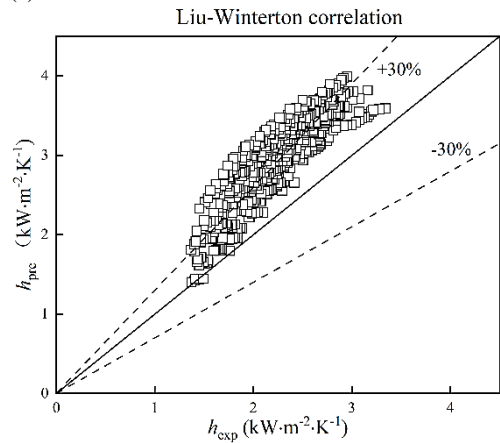
(b)
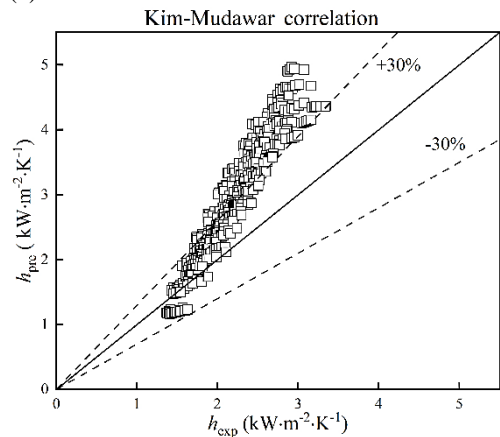
(c)

Fig. 5. Comparison of experimental data with correlations from the literature.

the full-threaded tube is dominated by the nucleate boiling, while that in the smooth tube and the front-threaded tube is dominated by the convective boiling. This is in agreement with the conclusion of existing studies (Dorao *et al.* 2018a) that heat transfer in smooth tubes of conventional size is dominated by the convective flow boiling. Although the heat transfer area of the front-threaded tube and the rear-threaded tube are identical, the heat transfer characteristics of the two tubes exhibit obvious differences. This confirms that the distribution of the internal thread structure has a significant influence on heat transfer.
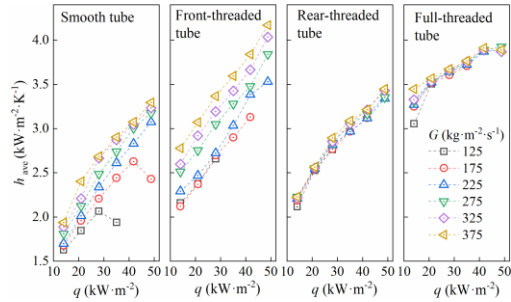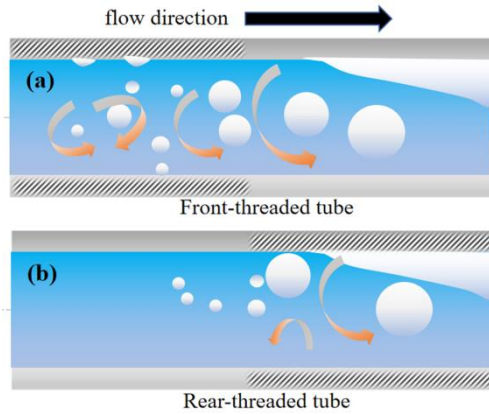

Fig. 6. Variation of the h_{ave} with the heat flux.

To further investigate the influence of segmented combination form on the heat transfer characteristics, the variations of h_{ave} with the mass flux for the four test tubes at different heat fluxes are compared, as shown in Fig. 7. The h_{ave} of the smooth tube and the front-threaded tube shows a gradual increase with increasing mass flux, while h_{ave} varies insignificantly for the rear-threaded tube and the full-threaded tube. As mentioned above, the heat transfer in the smooth tube and the front-threaded tube is dominated by convective boiling, and the increase of mass flux promotes the convection, thus improving the heat transfer. In contrast, the heat transfer in the rear-threaded tube and the full-threaded tube is mainly determined by the nucleate boiling. Herein, the effect of bubble nucleation and phase-change is stronger than that of convection, thus the h_{ave} is similar at different mass fluxes.
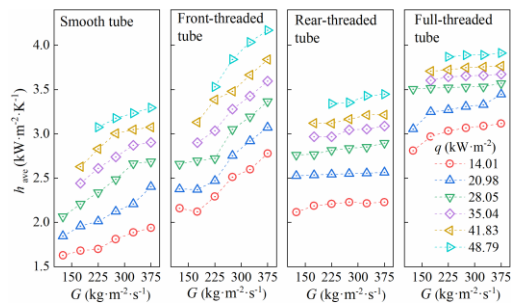
Fig. 7. Variation of the h_{ave} with the mass flux.

As mentioned before, for the internally-threaded tube, existing visualization studies have found that the nucleate bubbles were more likely to form in the groove of the micro-fin region (Yang and Hrnjak, 2020b). For the front-threaded tube, the internal thread structure in the front part will promote the bubble nucleation and the secondary flow, and these impacts could affect the whole test section along the flow direction, as shown in Fig. 8(a). Therefore, the corresponding enhanced convective disturbance dominates the heat transfer throughout the tube. For the rear-threaded tube, although the internal thread structure is also present, the secondary flow and nucleation enhancement mainly act in the rear half and fail to affect the whole test section as in the front-threaded tube, as shown in Fig. 8(b). Here, the effect of convection is weaker than the increase of nucleation sites, thus, the heat transfer is dominated by the nucleate boiling. For the full-threaded tube, the internal thread structure is distributed throughout the whole inner wall. The effect of the increased
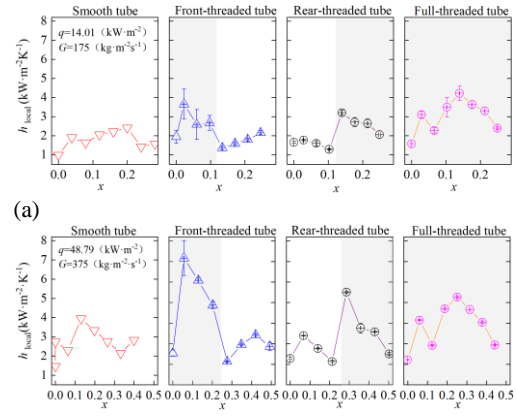
Fig. 8. Schematic diagram of the boiling mechanism of the test tubes.

(a)

(b)

Fig. 9. Variation of the h_{local} with the vapor quality along the path. (a) h_{local} at low *h*eat and mass flux. (b) h_{local} at high heat and mass flux.

nucleation sites is much greater than that of the secondary flow and other convective disturbances, and the heat transfer is thus dominated by the nucleate boiling. In summary, the heat transfer is enhanced when there are internal thread structures in the tube, but the heat transfer characteristics and the corresponding dominant heat transfer mechanism will change with the variation of the influence area and intensity of the strengthening effects.

Figure 9 shows the variations of local heat transfer coefficient (h_{local}) along the flow direction of the four tubes under the same operating conditions. The shaded parts marked in the figure correspond to the areas with the thread structure. It can be seen that h_{local} is higher in the first half and lower in the latter half for the front-threaded tube, while the corresponding pattern of change is reversed for the rear-threaded tube. The maximum h_{local} of the front and rear-threaded tube both appear in the section with thread structure, and are slightly lower than the maximum value for the full-threaded tube. Moreover, the h_{local} increases significantly for all four types of tubes at higher heat flux, as shown in Fig. 9(a) and Fig. 9(b), but the h_{local} of the tube with thread structure is still significantly higher than that of the smooth tube. The maximum values of h_{local} for the front and rear-threaded tubes also appear in the threaded region and have exceeded that of the full-threaded tube. Although the thread structure can significantly promote bubble nucleation and convection, the full-threaded tube generates excessive bubbles that can't be discharged in time at higher heat and mass fluxes, hindering the replenishment of the near-wall liquid working fluid, which in turn deteriorates the heat transfer performance.

4.2 Comparison of h_{ave} at high heat and mass fluxes

Figure 10 shows the three-dimensional plots of the average heat transfer coefficient for the four types of tubes at different heat and mass fluxes. It can be seen that h_{ave} of the smooth tube is lower among the four tubes, while h_{ave} of the full-threaded tube is overall higher. In addition, the heat transfer performance of the front-threaded tube is better than that of the full-threaded tube under high heat and mass flux conditions.
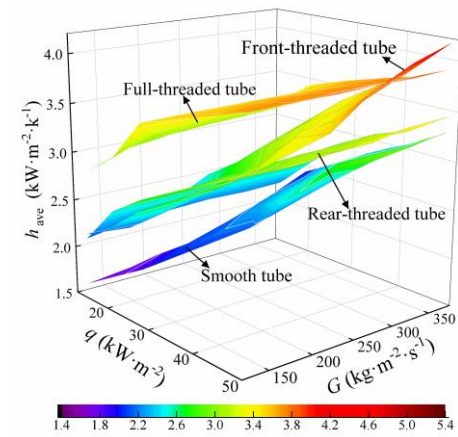
Fig. 10. Three-dimensional diagram of average heat transfer coefficients.

To further investigate the corresponding working characteristics, the heat transfer characteristics of the four tubes are compared at the highest heat flux and the highest mass flux, respectively, as shown in Fig. 11. It can be seen that the heat transfer coefficient increases with internal thread structures in the tube, but for the rear-threaded tube, the increase is limited. The possible reason is that the internal thread structure is in the rear half of the tube, which has a limited area of influence due to the flow direction. In contrast, the heat transfer enhancements are more pronounced for both the front-threaded tube and the full-threaded tube. In particular, h_{ave} of the front-threaded tube gradually exceeds that of the full-threaded tube as the heat flux and mass flux increase. This also indicates that the front-threaded tube has more advantages at high heat and mass fluxes, and the segmented distribution form of the internal thread has potential advantages.

To investigate the comprehensive performance of the segmented tube at high heat flux and high mass flux, PF' is defined as the ratio of pressure drop between segmented tube and full-threaded tube, EF' as the ratio of average heat transfer coefficient between segmented tube and full-threaded tube, and MF' as the ratio of EF' and PF'. The PF′, EF′ and MF′ of the front-threaded tube and the rear-threaded tube are

calculated and shown in Fig. 12, where the baseline indicates the full-threaded tube.

(a)

(b)
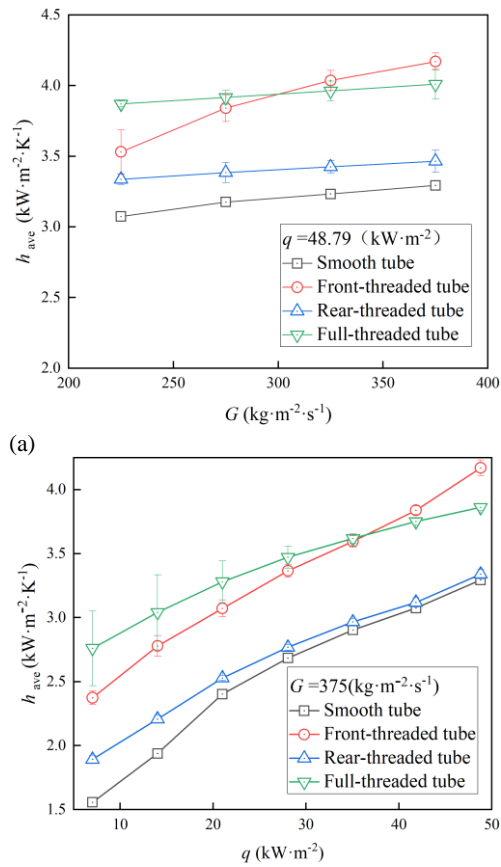
Fig. 11. The h_{ave} at the condition with high heat and mass fluxes. (a) h_{ave} at the highest heat flux. (b) h_{ave} at the highest mass flux.
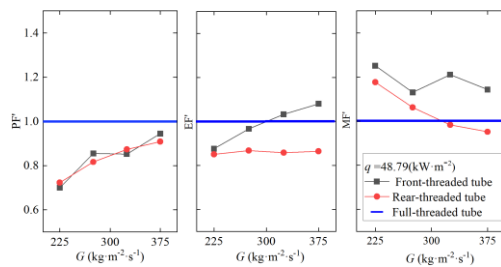
Fig. 12. Comparison of flow and heat transfer parameters based on full-threaded tubes.

As can be seen in Fig. 12, the pressure drops of the front-threaded tube and the rear-threaded tube are always lower than that of the full-threaded tube, which indicates the flow resistance of the full-threaded tube is indeed higher than others under the same conditions. For EF′, it can be found that the heat transfer capacity of the rear-threaded tube is always lower than that of the full-threaded tube, which is about 85 % of the latter. In contrast, the heat transfer capacity of the front-threaded tube gradually increases with the increase of the mass flux and eventually exceeds that of the full-threaded tube. Herein, the EF' of the front threaded tube reaches nearly 1.1 at the mass flux of 375 kW·m^{-2}·s^{-1}.

Finally, the comprehensive performance of the front-threaded tube is about 1.1 to 1.2 times higher than that of the full-threaded tube, which indicates that the energy consumption of the front-thread tube is lower under the same heat transfer enhancement effect.

5. CONCLUSION

In the present study, the flow boiling of R245fa in four types of tubes including smooth tube, front-threaded tube, rear-threaded tube, and full-threaded tube are studied experimentally. The main conclusions are as follows:

(1) The heat transfer is dominated by convective boiling in the smooth tube and front-threaded tube, and the heat transfer coefficients would increase significantly with increasing mass flux. In contrast, nucleate boiling dominates in the rear-threaded tube and the full-threaded tube, and the heat transfer performance almost keeps unchanged with the increase of the mass flux.

(2) Although the heat transfer areas of the front-threaded tube and the rear-threaded tube are the same, their heat transfer characteristics exhibit obvious differences. The reinforcing effect caused by the internal thread structure changes with the area and intensity, thus leading to the variation of the dominant mechanism of boiling heat transfer.

(3) It is found that at low heat flux and low mass flux, for h_{ave}, the order is: full threaded tube > front-threaded tube > rear-threaded tube > smooth tube; while at high heat flux and high mass flux, the order is: front-threaded tube > full-threaded tube > rear-threaded tube > smooth tube. Under the condition of high heat flux and high mass flux, the front-threaded tube shows a better comprehensive performance.

ACKNOWLEDGMENT

RERERENCES

Ali, R., B. Palm and M. H. Maqbool (2012). Flow Boiling Heat Transfer of Refrigerants R134a and R245fa in a Horizontal Micro-Channel. *Experimental Heat Transfer* 25(3), 181-196.

Charnay, R., R. Revellin and J. Bonjour (2014). Flow boiling characteristics of R-245fa in a minichannel at medium saturation temperatures. *Experimental Thermal and Fluid Science* 59, 184–194.

Ding, Y. J., J. H. Liu, L. Zhang and X. X. Yu (2020). Condensation heat transfer of R404A in horizontal inner-threaded tubes. *Journal of Engineering for Thermal Energy and Power* 35(12), 141-147

Dittus, F. W. and L. M. K. Boelter (1985). Heat transfer in automobile radiators of the tubular type. *International Communications in Heat and Mass Transfer* 12(1), 3–22.

Dorao, C. A., S. Drewes and M. Fernandino (2018a). Can the heat transfer coefficients for single-phase flow and for convective flow boiling be equivalent? *Applied Physics Letters* 112(6), 064101.

Dorao, C. A., F. Morin and M. Fernandino (2018b). Experimental Study of Nucleate Flow Boiling to Convective Flow Boiling Transition in a Horizontal Heated Pipe. *International Conference on Nanochannels, Microchannels, and Minichannels* 2018-7682.

Dastmalchi, M., A. Arefmanesh and G. A. Sheikhzadeh (2017). Numerical investigation of heat transfer and pressure drop of heat transfer oil in smooth and micro-finned tubes. *International Journal of Thermal Sciences* 121, 294-304.

Feng, L. L., K. Zhong, X. Xiao, H. W. Jia and X. Luo (2022). Experimental investigation on flow boiling characteristics of HFO-1234yf in a 0.5 mm microchannel. *International Journal of Refrigeration* 136, 71-81

Filho, E. and J. Jabardo (2014). Experimental study of the thermal hydraulic performance of sub-cooled refrigerants flowing in smooth, micro-fin and herringbone tubes. *Applied Thermal Engineering* 62(2), 461–469.

Gnielinski, V. (1975). *New equations for heat and mass transfer in the turbulent flow in pipes and channels*. NASA STI/Recon Technical Report A, 41, 8.

Hao, Q., J. Li and D. Geng (2020). Research on bubble behavior and heat transfer characteristics of flow boiling in rifled tubes. *Refrigeration* 48 (05), 59-65.

He, G., F. Liu, D. Cai and J. Jiang (2016). Experimental investigation on flow boiling heat transfer performance of a new near azeotropic refrigerant mixture R290/R32 in horizontal tubes. *International Journal of Heat and Mass Transfer* 102, 561–573.

He, K., J. Liu, L. Zhang and X. Yu (2019). Evaporation pressure drop characteristics of R404A in 5mm microfin tube. *Chemical Industry and Engineerng Progess* 38 (08), 3548-3555.

Jiang, G. B., J. T. Tan, Q. X. Nian, S. C. Tang and W. Q. Tao (2016). Experimental study of boiling heat transfer in smooth/micro-fin tubes of four refrigerants. *International Journal of Heat and Mass Transfer* 98, 631-642.

Jiang, J., G. He, Y. Liu, Y. Liu and D. Cai (2017). Flow boiling heat transfer characteristics and pressure drop of ammonia-lithium nitrate solution in a smooth horizontal tube.

International *Journal of Heat and Mass Transfer* 108, 220–231.

Kim, S. M. and I. Mudawar (2013). Universal approach to predicting saturated flow boiling heat transfer in mini/micro-channels – Part II. Two-phase heat transfer coefficient. International *Journal of Heat and Mass Transfer* 64, 1239–1256.

Liang, X., D. Cai, J. Deng and G. He (2019). Characteristics of boiling heat transfer and pressure drop of R410A in 5 mm diameter inner-grooved copper tubes. *Journal of Huazhong University of Science and Technology (Natural Science Edition)* 47 (03), 1-6.

Liu, Z. and R. H. S. Winterton (1991). A general correlation for saturated and subcooled flow boiling in tubes and annuli, based on a nucleate pool boiling equation. *International Journal of Heat and Mass Transfer* 34(11), 2759–2766.

Lu, Y., L. Zhao, S. Deng, D. Zhao and D. Wang (2020). Two phase flow pattern and heat transfer characteristics of R245fa / R134a under non-uniform heat flow. *Science China* 65 (17), 1741-1751.

Li, J. L., C. Z. Zhang., Q. Zhang and P. Yang (2022). Experimental investigation on onset of nucleate boiling and flow boiling heat transfer in a 5×5 rod bundle. *Applied Thermal Engineering* 208, 118263.

Liu, J., J. Liu and X. Xu (2020). Diabatic visualization study of r245fa two phase flow pattern characteristics in horizontal smooth and microfin tube. *International Journal of Heat and Mass Transfer* 152(5), 51301-51314.

Ma, H., G. Jiang and J. Bai (2011). Heat transfer characteristics of flow boiling in micro-fin tubes with R410A. *CIESC Journal* 62 (01), 41-46.

Moffat, R. J. (1988). Describing the uncertainties in experimental results. *Experimental Thermal and Fluid Science* 1(1), 3–17.

Mendoza-Miranda, J. M., A. Mota-Babiloni and J. Navarro-Esbr (2016). Evaluation of R448A and R450A as low-GWP alternatives for R404A and R134a using a micro-fin tube evaporator model. *Applied Thermal Engineering* 98, 330–339.

Ouyang, X., J. Chen and T. Li (2015). Boiling heat transfer performance in three internal enhanced tubes. *CIESC Journal* 66(6), 2076-2081.

Seo, K. and Y. Kim (2000). Evaporation heat transfer and pressure drop of R-22 in 7 and 9.52 mm smooth/micro-fin tubes. *International Journal of Heat and Mass Transfer* 43(16), 2869–2882.

Seol, H. K., I. C. Chu., M. H. Choi and D. J. Euh (2018). Mechanism study of departure of nucleate boiling on forced convective channel flow boiling. *International Journal of Heat and Mass Transfer* 126, 1049–1058.

Subhanker, P., M. Fernandinoa and C. A. Dorao (2021). On the scaling of convective boiling heat transfer coefficient. *International Journal of Heat and Mass Transfer* 164, 120589.

Solanki, A. K. and R. Kumar (2018). Condensation of R-134a inside micro-fin helical coiled tube-in-shell type heat exchanger. *Experimental Thermal and Fluid Science* 93, 344-355.

Targanski, W. and J. T. Cieslinski (2007). Evaporation of R407C/oil mixtures inside corrugated and micro-fin tubes. *Applied Thermal Engineering* 27(13), 2226–2232.

Yoshida, S., H., Mori, H. Hong and T. Matsunaga (2011). Prediction of Heat transfer coefficient for refrigerants flowing in horizontal evaporator tubes. *Transactions of the Japan Society of Refrigerating and Air Conditioning Engineers* 11, 67.

Yang, C. M. and P. Hrnjak (2018). Effect of straight micro fins on heat transfer and pressure drop of R410A during evaporation in round tubes. *International Journal of Heat and Mass Transfer* 117, 924–939.

Yang, C. M. and P. Hrnjak (2019). Effect of helical micro-fins on two-phase flow behavior of R410A evaporating in horizontal round tubes obtained through visualization. *International Journal of Heat and Mass Transfer* 144, 118654.

Yang, C. M. and P. Hrnjak (2020a). A new flow pattern map for flow boiling of R410A in horizontal micro-fin tubes considering the effect of the helix angle. *International Journal of Refrigeration* 109, 154-160.

Yang, C. M. and P. Hrnjak (2020b). Diabatic visualization shows effects of micro-fins on evaporation of R410A: Smooth, axial micro-fin, and helical micro-fin tubes. *International Journal of Heat and Mass Transfer* 150, 119276.

Yu, X. X., J. H. Liu, K. He and H. Y. Wang (2019). Study on the Flow Boiling Heat Transfer Characteristics of R404A in 5 mm Micro-fin Tube. *Journal of Engineering for Thermal Energy and Power* 10, 16146.

Zhao, X. and P. Bansal (2012). Flow boiling heat transfer analysis of new experimental data of CO2 in a micro-fin tube at −30 °C. *International Journal of Thermal Sciences* 59, 38–44.